Single-walled Carbon Nanotube Film as Electrode in Indium-free Planar Heterojunction Perovskite Solar Cells: Investigation of Electron-blocking Layers and Dopants

Il Jeon,[†] Takaaki Chiba,[‡] Clement Delacou,[‡] Yunlong Guo,[†] Antti Kaskela,[§] Olivier Reynaud,[§] Esko I. Kauppinen,[§] Shigeo Maruyama,[‡] and Yutaka Matsuo[†]*

†: Department of Chemistry, School of Science, The University of Tokyo, 7-3-1 Hongo, Bunkyo-ku, Tokyo 113-0033, Japan

‡: Department of Mechanical Engineering, School of Engineering, The University of Tokyo, 7-3-1 Hongo, Bunkyo-ku, Tokyo 113-8656, Japan

§: Department of Applied Physics, Aalto University School of Science, 15100, FI-00076 Aalto, Finland

Abstract: In this work, we fabricated indium-free perovskite solar cells (SCs) using direct- and dry-transferred aerosol single-walled carbon nanotube (SWNT). We investigated diverse methodologies to solve SWNT's hydrophobicity and doping issues in SC devices. These include changing wettability of poly(3,4-ethylenedioxythiophene)/poly(styrenesulfonate) (PEDOT:PSS), MoO_3 thermal doping, and HNO_3(aq) doping with various dilutions from 15 to 70 v/v% to minimize its instability and toxic nature. We discovered that isopropanol (IPA) modified PEDOT:PSS works better than surfactant modified PEDOT:PSS as an electrode in perovskite SCs due to superior wettability, while MoO_3 is not compatible owing to energy level mismatching. Diluted HNO_3 (35 v/v%)-doped SWCNT-based device performed the highest PCE of 6.32% among SWNT-based perovskite SCs, which is 70% of an indium tin oxide (ITO)-based device (9.05%). Its flexible application showed 5.38% on a polyethylene terephthalate (PET) substrate.

Recent emergence of perovskite solar cells have drawn much attention on account of high PCE arising from a long exciton diffusion length of around 100 nm, high absorption coefficient and carrier mobility, and a suitable band gap of around 1.55 eV.[1-4] Since Miyasaka reported a prototype perovskite-based dye-sensitized solar cell[5], perovskite SCs have been making a remarkable advancement and now the PCEs reach around 20%.[6-8] Similarly, organic SCs have also drawn attention for its low-cost, lightweight, and chemically modifiable nature. However, ITO is indispensible in both types of SCs and its use potentially brings about problems such as lack of supply for mass production and imperfect flexibility for wearable applications.

As an ITO replacement, SWNTs have been regarded promising for their mechanical flexibility, abundant carbon composition, easy synthesis, and direct roll-to-roll processability.[9] SWNTs are structurally the simplest class of carbon nanotubes and its architecture can be described as a single graphene rolled in a cylindrical shape with typical diameters in the range of 0.4–3.0 nm.[10] Following the independent discoveries by Iijima in early 1990s, research on its synthesis and properties accelerated greatly.[11] Recently, the high quality free-standing purely single-walled carbon nanotubes, which are directly transferrable by aerosol chemical vapor deposition, have been developed.[12] This technique can produce SWNT with the transparency of over 90% and the resistance of around 85 Ωcm^{-2}. Its synthetic process is better than the other conventional methods which suffer from resource-consuming liquid dispersion and purification steps ending up with dense SWNT networks.[13-15] The success of SWNT application in photovoltaics depends on two things: its effective doping in a manner that the dopant does not undermine device performance and overcoming the intrinsic hydrophobicity of SWNTs for uniform film fabrication.

So far, SWNT electrode for organic SCs have been reported in great amount[16-24] and the PCE has been reported to reach as high as 83% to that of ITO counterpart.[25] Yet, analogue applications in perovskite SCs have not been reported to date. SWNT electrode application was limited only to metal electrode replacement.[26] Besides, other flexible perovskite SCs reported utilize flexible ITO which suffers from many shortcomings such as low conductivity and crack-damage when bent too much.[27, 28]

Here we report SWNT-based indium-free perovskite SCs and flexible application along with investigations of different charge selective layers and doping methods which overcome the issues of doping and hydrophobicity of SWNT films. A planar heterojunction structure was used in this study which comprises of PEDOT:PSS as an electron-blocking layer (EBL), followed by

perovskite layer ($CH_3NH_3PbI_3$), [6,6]-phenyl C61-butyric acid methyl ester ($PC_{61}BM$), and an aluminum metal electrode. This was coined by Snaith as "inverted cell architecture".[29] Although mesoporous (mp)-TiO_2-based perovskite SC exhibits a higher PCE, the formation of mp-TiO_2 layer requires a thermal process over 450 °C. Since flexible substrates are vulnerable to high temperature, the inverted planar heterojunction perovskite SC, which requires annealing temperature lower than 100 °C, was regarded more promising for our flexible applications.[30-32] Furthermore, this structure demonstrates better stability under ultraviolet light[33] and almost no hysteresis with sweep directions in measurement because of the exclusion of mp-TiO_2.[34, 35] One-step solution method, which is the most widely established[36], was employed in this work as we focused on achieving reliable investigation prior to a record-breaking PCE.

SWNT perovskite SC devices using modified PEDOT:PSS. One of the challenges for SWNT electrode-based solar cells has been doping the carbon nanotube while having a desirable EBL function. PEDOT:PSS with acidic nature functions as both the EBL and dopant.[37] However, hydrophilic PEDOT:PSS cannot be applied directly onto hydrophobic SWNTs. As a solution to this problem, we selected two approaches: firstly diluting PEDOT:PSS in IPA solvent by 1:3 (v/v) ratio,[38] or adding a small amount (0.5 wt%) of surfactant, polyoxyethylene(6) tridecyl ether to the PEDOT:PSS solution.[39] These two are already well-established methods in the application of graphene and inverted organic SCs, respectively. These modifications change PEDOT:PSS property from hydrophilic to hydrophobic. In the case of planar graphene sheet, modified PEDOT:PSS cannot form a complete coverage, and deposition of additional MoO_3 is mandatory.[40] But, in the case of carbon nanotube, both IPA-modified PEDOT:PSS (IPA-PEDOT:PSS) and surfactant-modified PEDOT:PSS (surfactant-PEDOT:PSS) thoroughly over-coated the individual tubes as evidenced by scanning electron microscopy (SEM) images (Figure

1 b and c). Knowing that the SWNT films do not have shunt pathways, planar heterojunction perovskite SCs were fabricated without an additional MoO_3 layer. During the fabrication, specifically when spin coating a perovskite layer, it was interesting to observe formation of discontinuous large crystals in the perovskite layer on the surfactant-PEDOT:PSS-coated SWNT (Figure S1). The cross-sectional SEM reveals a bad uniformity of the perovskite layer. Those unwanted crystals could be avoided by shortening the chlorobenzene (CB) rinsing time from the usual 10 to 6 sec. From atomic force microscopy (AFM) images and their roughness average values (Ra), it is visible that the surfactant-PEDOT:PSS-coated SWNT had rougher morphology than the IPA-PEDOT:PSS-coated SWNT (Figure 1 f and g). The perovskite layers formed on top of those films shows even bigger difference (Figure 1 j and k). Both AFM images of the modified-PEDOT:PSS-based perovskite shows bigger crystal size and rougher surface than the reference perovskite layer (Figure 1 j, k and i).
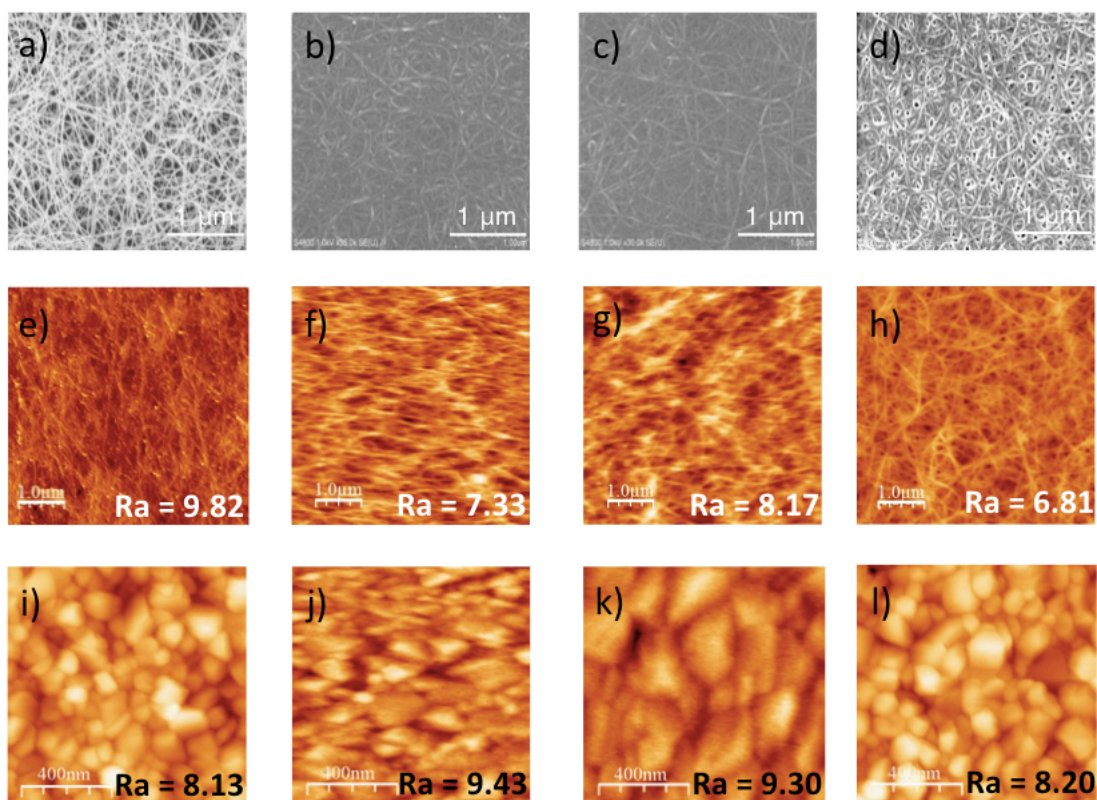
Figure 1. SEM images of a) SWNTs, b) IPA-PEDOT:PSS on SWNTs, c) Surfactant-PEDOT:PSS on SWNTs, d) PEDOT:PSS on HNO$_3$-doped SWNTs; AFM images and r.m.s. roughness values of e) SWNTs, f) IPA-PEDOT:PSS on SWNTs, g) Surfactant-PEDOT:PSS on SWNTs, h) PEDOT:PSS on HNO$_3$-doped SWNTs, i) perovskite layer on PEDOT:PSS on ITO, j) perovskite layer on IPA-PEDOT:PSS on SWNTs, k) perovskite layer on Surfactant-PEDOT:PSS on SWNTs, and l) perovskite layer on PEDOT:PSS on HNO$_3$-doped SWNTs.

According to Table 1, the IPA-PEDOT:PSS-applied SWNT-based perovskite SC performed better than the surfactant-PEDOT:PSS-applied SWNT-based perovskite SC. (Device 2 and Device 3, respectively) The short-circuit current density (J_{SC}) values were similar, but the open circuit voltage (V_{OC}) and the fill factor (FF) in the IPA-PEDOT:PSS-based device were higher than the surfactant-PEDOT:PSS-based device. Similar J_{SC} meant that their exciton dissociation and extraction were okay. But lower V_{OC} and shunt resistance (R_{SH}) indicated that the PEDOT:PSS coverage was the problem. Figure S2 shows observation of the IPA-PEDOT:PSS

and the surfactant-PEDOT:PSS as cast, and water contact angle test results. The IPA-PEDOT:PSS on SWNT shows a complete coverage on the substrate (Fig S2 a), yet the surfactant-PEDOT:PSS barely soaked SWNT and could not expand to the glass part (Fig S2 b). Compared to the IPA-PEDOT:PSS solution, the surfactant-PEDOT:PSS solution is less hydrophilic.

As it has been proposed that the lower performance of perovskite SCs arises from pin-hole formation and incomplete coverage of the perovskite,[41-43] inconsistently de-wetted PEDOT:PSS surface will aggravate perovskite crystals because of perovskite layer's thermodynamic instability as predicted from energetic standpoint.[44] CB reduces the solubility of $CH_3NH_3PbI_3$ by removing the first solvent, thereby promoting fast nucleation and growth of the crystals. Therefore, the CB rinsing time had to be shortened for the surfactant-PEDOT:PSS applied SWNT to avoid the crystal aggregations. Nevertheless, shortening the rinsing time induced premature crystallization, which undercut the device performance. This explains why the surfactant-PEDOT:PSS-applied SWNT based device performed badly while the surfactant-PEDOT:PSS-applied on ITO, which has flatter morphology than SWNT, gave a higher PCE (Table S1).

Table 1. Photovoltaic performance table for SWNT perovskite SCs using modified PEDOT:PSS and a range of SWNTs with different HNO_3 concentrations. Corresponding *J-V* curves are shown in Figure S3.

Device	Electrode	EBL	V_{OC} (V)	J_{SC} (mA/cm^2)	FF	R_S (Ωcm^2)	R_{SH} (Ωcm^2)	PCE (%)
1	ITO	PEDOT:PSS	0.83	16.3	0.64	25.8	5.2 x 10^5	9.05
2	SWNT	IPA-PEDOT:PSS	0.77	11.1	0.50	53.7	2.7 x 10^3	4.27
3	SWNT	Surfactant-PEDOT:PSS	0.61	11.8	0.38	40.9	1.2 x 10^3	2.71
4	70 v/v% HNO$_3$-SWNT		0.77	14.4	0.55	79.2	5.7 x 10^3	6.09
5	50 v/v% HNO$_3$-SWNT	PEDOT:PSS	0.76	14.5	0.52	86.0	2.5 x 10^3	5.84
6	35 v/v% HNO$_3$-SWNT		0.79	14.9	0.54	94.1	4.8 x 10^3	6.32
7	15 v/v% HNO$_3$-SWNT		0.77	13.6	0.39	122	1.8 x 10^3	3.88

Using 4-point probe measurement, resistivity of various SWNTs was measured (Table 2). The IPA-PEDOT:PSS SWNT displayed higher sheet resistance (R_{Sheet}) than the surfactant-PEDOT:PSS. This is due to a relatively large amount of IPA-PEDOT:PSS dilution, which is 1:3 in volume to volume ratio. Its influence is reflected from the higher series resistance (R_S) value of Device 2 (Table 1). Nevertheless, overall, the IPA-PEDOT:PSS is more compatible with SWNT films in perovskite SCs than the surfactant-PEDOT:PSS because of its favored wettability.

Table 2. Conductivity of ITO/PEDOT:PSS, SWNT/modified-PEDOT:PSS, SWNT/Surfactant-PEDOT:PSS, and SWNTs doped with different HNO_3 concentrations measured by 4-point probe measurement.

Electrode	EBL	R_{Sheet} (Ω)
ITO	PEDOT:PSS	9.8
SWNT	IPA-PEDOT:PSS	208.2
SWNT	Surfactant-PEDOT:PSS	109.6
70 v/v% HNO_3-SWNT	PEDOT:PSS	23.7
50 v/v% HNO_3-SWNT		28.3
35 v/v% HNO_3-SWNT		25.6
15 v/v% HNO_3-SWNT		38.6

Water diluted nitric acid-doped SWNT soaked by pristine PEDOT:PSS as an electrode in perovskite SCs. The compatibility of SWNTs with PEDOT:PSS can be improved by doping SWNTs with HNO_3 which changes SWNT's property from hydrophobic to hydrophilic. This also entails strong doping effect due to strongly acidic nature of HNO_3. Nitric acid doping serves as the most effective dopant to date. However, it is toxic and highly reactive.[45] Therefore, HNO_3 was diluted to the extent that its lethal effect is minimized while its doping effective is still retained. It was reported that the greater the acid concentration, the greater the doping effect, but too highly concentrated acid can damage SWNTs.[46, 47] Accordingly, we investigated the relationship between acid concentrations and device performance.

HNO$_3$ doping on SWNT films was achieved by applying one drop of HNO$_3$(aq) and drying at 90 °C for 10 min. HNO$_3$ doping made SWNTs hydrophilic enough to allow formation of a fine layer of unmodified PEDOT:PSS on top (Figure 1 d). The AFM images and Ra roughness values reveals uniform PEDOT:PSS-soaked SWNT compared to the modified PEDOT:PSS-soaked SWNT (Figure 1 f, g, and h). Indeed, high V_{OC} and R_{SH} values of Device 4 (Table 1) show us that there is no shunt pathway created between the perovskite layer and the SWNT electrode. These values are higher than those of the devices fabricated using the modified PEDOT:PSS-soaked SWNT electrodes.[48, 49] Perovskite films show nice morphology as good as the reference too (Figure 1 i and l). We attribute this to the uniformity of the electrode as well the use of unmodified PEDOT:PSS.

Device performances of the HNO$_3$-doped SWNT-based perovskite SCs with different HNO$_3$ concentrations were compared (Table 1, Device 4–7). We could observe that all of the HNO$_3$-doped SWNTs-based perovskite SCs showed much higher PCEs than those of the modified PEDOT:PSS-based SWNTs. The high performance can be attributed to the improved J_{SC}, which is due to enhanced transmittance of SWNT films by the acid doping. It must be mentioned that strong 70 v/v% HNO$_3$ did not destroy nor undermine the device performance (Device 4). In addition, there was no stark difference in PCEs between acid concentrations except for 15 v/v% in which the PCE dropped to 3.88% (Device 7).

UV-vis spectroscopy and Raman spectroscopy were measured to confirm and compare the transparency and the doping effect. Figure 2 a) shows spectra of HNO$_3$-doped SWNTs having subdued Van Hove peaks (M_{11}, E_{22}, E_{11}) which is an indication of successful doping. The transmittance spectrum of the SWNT doped by HNO$_3$ (15 v/v%) was lower than the other samples doped by HNO$_3$ with higher concentrations. This shows that the 15 v/v% HNO$_3$

possesses weaker doping effect than the rest. Raman spectra (Figure 2 b) followed the same trend: all of the HNO_3-doped SWNTs, except 15 v/v%-concentrated sample exhibited the G-band shifts. Yet, the HNO_3 (15 v/v%)-doped SWNT film's doping effect was stronger than the SWNT film treated by IPA-PEDOT:PSS which showed a slightly higher transmittance than the untreated SWNT film in the UV-vis spectra while showing no shift in Raman spectra. Conductivity measurement also revealed higher resistivity of HNO_3 (15 v/v%)-doped SWNT (Table 2). It can be concluded that HNO_3 (35 v/v%) is the optimum concentration for the application in SWNT-based perovskite SCs.
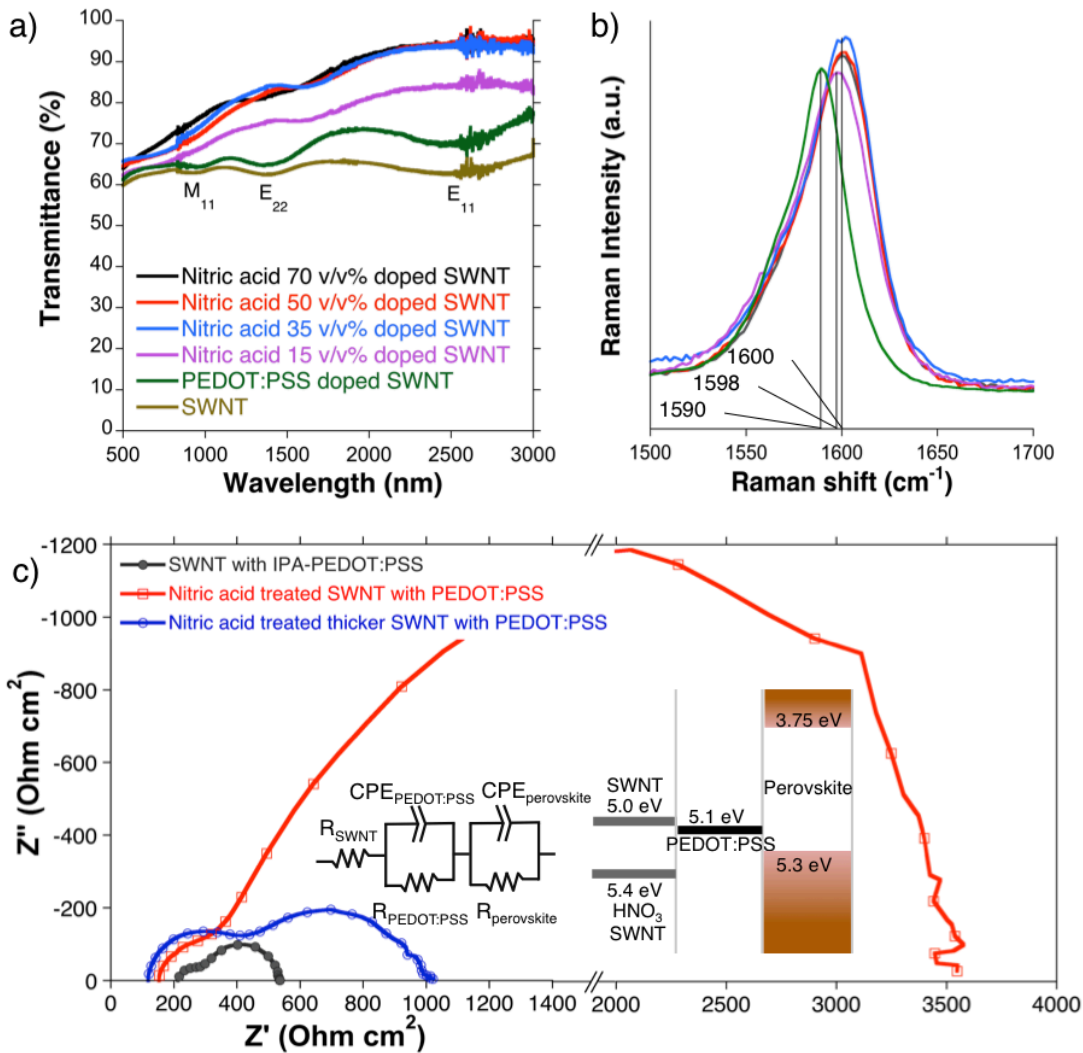
Figure 2. Transmittance (a) and Raman shift values (b) of HNO_3-doped SWNT films with different acid concentrations, an IPA-PEDOT:PSS-soaked SWNT film and an untreated SWNT film using UV-vis spectroscopy and Raman spectroscopy, respectively. Both spectra share the same legend. (c) Nyquist plot of perovskite SCs with IPA-PEDOT:PSS-applied SWNT, HNO_3-doped (treated) SWNT, and HNO_3-doped (treated) thicker SWNT measured at 0 mV applied bias under dark condition; the equivalent circuit and the band diagram are shown in the inset.

Another fascinating point about HNO_3-doped SWNTs in perovskite SCs is that R_S values were rather high considering their low R_{Sheet} in Device 4 to 7 (Table 2). This phenomenon was not observed in organic SCs.[16] Therefore, we employed a thicker SWNT film (65% transmittance at

550 nm wavelength) and fabricated a device expecting lower R_S, because thicker SWNT films possess lower resistance intrinsically. However, the HNO_3-doped thicker SWNT-based perovskite SC did not improve R_S (Table S1). To find out the reason behind this, impedance measurements were carried out. Spectra at 0 mV in dark condition are shown in Figure 2 c). The data reveal that HNO_3-doped SWNT-based perovskite SCs possesses much higher electrical boundaries than the IPA-PEDOT:PSS-treated SWNT, despite low R_{Sheet} in both thinner and thicker SWNT films. The Fermi levels of SWNTs measured by Kelvin probe force microscopy indicated that HNO_3-doped SWNTs' Fermi levels were 5.4 eV for all of the HNO_3 concentrations, while pure SWNT's Fermi level sat at 5.0 eV.[50] It can be concluded that the HNO_3-doped SWNT films provide relatively less driving force for the hole injection from the perovskite layer and this causes higher R_S. Indeed, if we compare the energy band diagrams of SWNT-based perovskite SCs and organic SCs, we can understand that the organic SCs are energetically more favored. (Figure S4)

Introduction of MoO_3 in perovskite SCs. MoO_3 as an EBL has been commonly used in place of PEDOT:PSS in organic SCs. In fact, MoO_3 is preferred over acidic PEDOT:PSS.[51] However, the same usage has not been witnessed in the field of perovskite SCs. It can be presumed that this is due to its incompatibility in perovskite SCs, but no clear account has been given so far. Since it was reported that thermally annealing MoO_3 can dope SWNTs in a safe and effective manner, we were compelled to study its compatibility in SWNT-based perovskite SCs.[52]

Table 3 and Table S2 show diverse configurations of perovskite SCs using MoO_3. It reveals that MoO_3-applied perovskite SCs performed poorly on both ITO (Table 1: Device A) and SWNT film (Table 1: Device B). When PEDOT:PSS and MoO_3 combinations were used in hopes of improving the interface morphology, the photovoltaic parameters did not improve (Table S2). Moreover, we thermally annealed MoO_3 above and/or below SWNTs in order to dope SWNT. This process reduces oxygen stoichiometry of MoO_3 to MoO_x where x is a number between 2 and 3. The PCEs improved only a little (Table 1: Device C).

Table 3. Photovoltaic performance table for inverted planar heterojunction SWNT perovskite SCs and normal planar heterojunction ITO perovskite SCs using MoO_3 layers in various structural configurations. Corresponding *J-V* curves are shown in Figure S5-1.

Device	Anode	V_{OC} (V)	J_{SC} (mA/cm^2)	FF	PCE (%)
A	ITO/MoO$_3$	0.46	0.64	0.42	0.12
B	SWNT/MoO$_3$	0.37	0.51	0.28	0.05
C	SWNT/MoO$_x$/PEDOT:PSS	0.58	13.0	0.42	2.09
	Cathode				
D	spiro-MeOTAD/Ag	0.96	21.0	0.68	13.7
E	spiro-MeOTAD/MoO$_3$/Ag	0.85	12.6	0.21	2.22
F	MoO$_3$/Ag	0.48	2.01	0.32	0.30

As the quality of perovskite layers were visually fine during the fabrication, energy mismatching was suspected to be the root of this incompatibility. Photoluminescence spectroscopy and impedance measurements were carried out to investigate this. Photoluminescence quenching is a well established method demonstrating charge extraction

ability of EBL in contact with perovskite.[29] Figure 3a shows that photoluminescence of halide methylammonium lead perovskite was reduced strongly when it was next to PEDOT:PSS, but not when it was next to either ITO or MoO_3.[53] According to Figure 3b, the electronic boundary between perovskite and MoO_3 was too big that it made a complete vertical line. The Fermi level of MoO_3 was measured using photoelectron yield spectroscopy. It indicated that MoO_3 had the Fermi level of around 6.0 eV. Thermal annealing dropped this value to 7.0 eV. As valence band of perovskite is around 5.3 eV, there is energy level mismatch with MoO_3. On the contrary, PEDOT:PSS had the Fermi level at around 5.1 eV. Therefore the hole transfer is not hindered between perovskite and PEDOT:PSS. In the case of organic acceptors like $PC_{61}BM$, its HOMO (6.01 eV) lies much lower than the valence band of the perovskite. (Figure 3b inset) This explains why MoO_3 is compatible in organic SCs but incompatible in perovskite SCs.
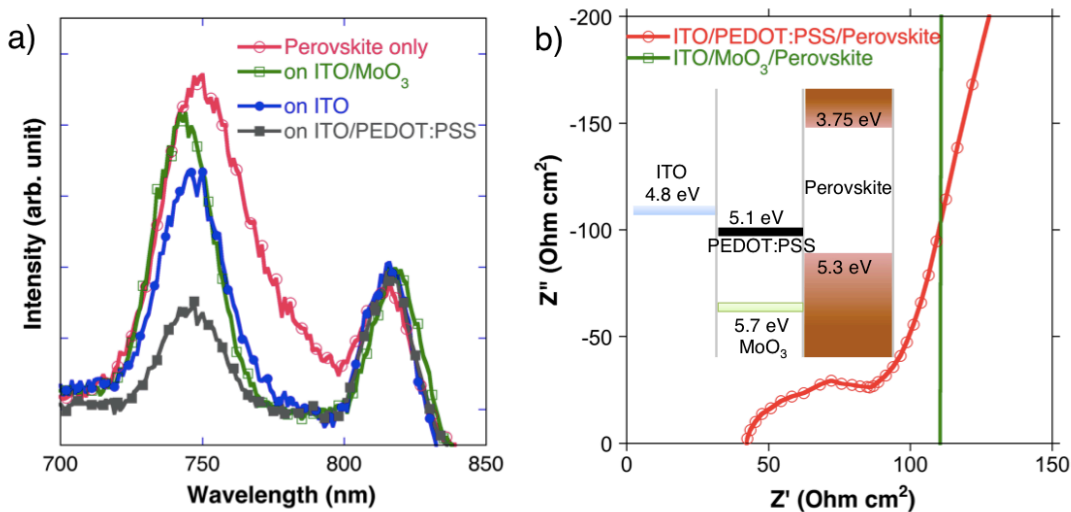

Figure 3. a) Photoluminescence spectra of a perovskite layer only, a perovskite film on a MoO_3 film on an ITO glass, a perovskite film on an ITO glass, and a perovskite film on a PEDOT:PSS film on an ITO glass; b) Nyquist plot of perovskite SCs with a PEDOT:PSS film on an ITO glass and a MoO_3 film on an ITO glass measured at 0 mV applied bias under dark condition; the band diagram is shown in the inset.

In spite of the incompatibility of MoO_3 in inverted type perovskite SCs, there are some reports on normal type perovskite SCs utilizing MoO_3 as an EBL.[54, 55] In order to verify, we fabricated normal type planar heterojunction perovskite SCs using MoO_3. Device D in Table 3 (glass/ITO/TiO_2/perovskite/spiro-MeTAD/Ag) showed a descent performance of a typical normal type perovskite SC using spiro-MeOTAD. When MoO_3 was inserted next to spiro-MeOTAD, it decreased the PCE greatly. When only MoO_3 was used as an EBL, its performance was even worse and these results support our assertion.

Flexible applications of SWNT perovskite SCs. The best performing configuration from this study was chosen and perovskite SCs were fabricated on a flexible polyethylene terephthalate (PET) substrate (HNO_3 (35 v/v%)-doped SWCNT-based device). A cyclic flex test with a curvature of 10 mm was imposed to check the resilience (Table S3). A PCE of 5.38% with a V_{OC} of 0.71 V, J_{SC} of 11.8 mAcm^{-2}, and fill factor of 0.56 under AM1.5 100 mWcm^{-2} illumination was achieved. After the severe flex cyclic test, the performance dropped a little (4.60%), but it retained its diode character well enough. Pictures and a cross sectional SEM image is shown in Figure S8.

In summary, the three mainstream approaches to SWNT application in perovskite SCs had been viewed. Their compatibility, effectiveness, and mechanism had been studied to understand the uniqueness of perovskite SCs. Modified PEDOT:PSS worked fairly well but the PCEs were limited. Application of MoO_x on the other hand was not compatible in perovskite SCs, much to our surprise. HNO_3-doped SWNTs were the best performing even in its diluted form up to 35 v/v%, yet its mobility was marginally hindered by the energy level difference between highly lying perovskite valence band and strongly p-doped SWNT electrode's Fermi level. Using this approach, we achieved a flexible ITO-free planar heterojunction perovskite SC device with a

PCE of 5.38% which is 60% of ITO reference device (9.05%). As non-ITO and SWNT-based perovskite SCs, we anticipate this work can initiate and contribute to the development of ITO-free perovskite SC research. We anticipate these findings will provide better understanding of carbon nanotube application as a transparent conductive electrode in ITO-free perovskite solar cells.

ASSOCIATED CONTENT

Supporting Information: Experimental procedures, more cross-section and top view SEM data, hydrophobicity observation, J-V curves, etc. This material is available free of charge via the Internet at http://pubs.acs.org.

AUTHOR INFORMATION

Corresponding Author

*matsuo@chem.s.u-tokyo.ac.jp

Notes

The authors declare no competing financial interest.

REFERENCES

1.   Lee, M. M.; Teuscher, J.; Miyasaka, T.; Murakami, T. N.; Snaith, H. J. *Science* **2012,** 338, (6107), 643-7.

2.   Noh, J. H.; Im, S. H.; Heo, J. H.; Mandal, T. N.; Seok, S. I. *Nano Lett* **2013,** 13, (4), 1764-9.

3.   Heo, J. H.; Im, S. H.; Noh, J. H.; Mandal, T. N.; Lim, C.-S.; Chang, J. A.; Lee, Y. H.; Kim, H.-j.; Sarkar, A.; Nazeeruddin, M. K.; Grätzel, M.; Seok, S. I. *Nature Photonics* **2013,** 7, (6), 486-491.

4.   Liu, M.; Johnston, M. B.; Snaith, H. J. *Nature* **2013,** 501, (7467), 395-8.

5.   Kojima, A.; Teshima, K.; Shirai, Y.; Miyasaka, T. *Journal of the American Chemical Society* **2009,** 131, (17), 6050-6051.

6.   McGehee, M. D. *Nat Mater* **2014,** 13, (9), 845-6.

7.   Park, N.-G. *The Journal of Physical Chemistry Letters* **2013,** 4, (15), 2423-2429.

8.   Kazim, S.; Nazeeruddin, M. K.; Gratzel, M.; Ahmad, S. *Angew Chem Int Ed Engl* **2014,** 53, (11), 2812-24.

9.   De Volder, M. F. L.; Tawfick, S. H.; Baughman, R. H.; Hart, A. J. *Science* **2013,** 339, (6119), 535-539.

10.   Hatton, R. A.; Miller, A. J.; Silva, S. R. P. *Journal of Materials Chemistry* **2008,** 18, (11), 1183.

11.   Iijima, S.; Ichihashi, T. *Nature* **1993,** 363, (6430), 603-605.

12.   Kaskela, A.; Nasibulin, A. G.; Timmermans, M. Y.; Aitchison, B.; Papadimitratos, A.; Tian, Y.; Zhu, Z.; Jiang, H.; Brown, D. P.; Zakhidov, A.; Kauppinen, E. I. *Nano Lett* **2010,** 10, (11), 4349-55.

13.   Zhou, Y.; Hu, L.; Grüner, G. *Applied Physics Letters* **2006,** 88, (12), 123109.

14.   Lim, C.; Min, D.-H.; Lee, S.-B. *Applied Physics Letters* **2007,** 91, (24), 243117.

15.   Wu, Z.; Chen, Z.; Du, X.; Logan, J. M.; Sippel, J.; Nikolou, M.; Kamaras, K.; Reynolds, J. R.; Tanner, D. B.; Hebard, A. F.; Rinzler, A. G. *Science* **2004,** 305, (5688), 1273-1276.

16.   Du, J.; Pei, S.; Ma, L.; Cheng, H. M. *Adv Mater* **2014,** 26, (13), 1958-91.

17.   Unalan, H. E.; Hiralal, P.; Kuo, D.; Parekh, B.; Amaratunga, G.; Chhowalla, M. *Journal of Materials Chemistry* **2008,** 18, (48), 5909.

18.   Tanaka, H.; Yasuda, T.; Fujita, K.; Tsutsui, T. *Advanced Materials* **2006,** 18, (17), 2230-2233.

19.   Kim, Y. H.; Müller-Meskamp, L.; Zakhidov, A. A.; Sachse, C.; Meiss, J.; Bikova, J.; Cook, A.; Zakhidov, A. A.; Leo, K. *Solar Energy Materials and Solar Cells* **2012,** 96, (0), 244-250.

20.   Tyler, T. P.; Brock, R. E.; Karmel, H. J.; Marks, T. J.; Hersam, M. C. *Advanced Energy Materials* **2011,** 1, (5), 785-791.

21.   Salvatierra, R. V.; Cava, C. E.; Roman, L. S.; Zarbin, A. J. G. *Advanced Functional Materials* **2013,** 23, (12), 1490-1499.

22.   Cui, K.; Anisimov, A. S.; Chiba, T.; Fujii, S.; Kataura, H.; Nasibulin, A. G.; Chiashi, S.; Kauppinen, E. I.; Maruyama, S. *J. Mater. Chem. A* **2014,** 2, (29), 11311-11318.

23.   Dabera, G. D. M. R.; Jayawardena, K. D. G. I.; Prabhath, M. R. R.; Yahya, I.; Tan, Y. Y.; Nismy, N. A.; Shiozawa, H.; Sauer, M.; Ruiz-Soria, G.; Ayala, P.; Stolojan, V.; Adikaari, A. A. D. T.; Jarowski, P. D.; Pichler, T.; Silva, S. R. P. *ACS Nano* **2013,** 7, (1), 556-565.

24.   Kim, S.; Yim, J.; Wang, X.; Bradley, D. D. C.; Lee, S.; deMello, J. C. *Advanced Functional Materials* **2010,** 20, (14), 2310-2316.

25.   .

26.   Li, Z.; Kulkarni, S. A.; Boix, P. P.; Shi, E.; Cao, A.; Fu, K.; Batabyal, S. K.; Zhang, J.; Xiong, Q.; Wong, L. H.; Mathews, N.; Mhaisalkar, S. G. *ACS Nano* **2014,** 8, (7), 6797-6804.

27.   Kim, B. J.; Kim, D. H.; Lee, Y.-Y.; Shin, H.-W.; Han, G. S.; Hong, J. S.; Mahmood, K.; Ahn, T. K.; Joo, Y.-C.; Hong, K. S.; Park, N.-G.; Lee, S.; Jung, H. S. *Energy Environ. Sci.* **2015,** 8, (3), 916-921.

28.   You, J.; Hong, Z.; Yang, Y.; Chen, Q.; Cai, M.; Song, T.-B.; Chen, C.-C.; Lu, S.; Liu, Y.; Zhou, H.; Yang, Y. *ACS Nano* **2014,** 8, (2), 1674-1680.

29.   Docampo, P.; Ball, J. M.; Darwich, M.; Eperon, G. E.; Snaith, H. J. *Nat Commun* **2013,** 4, 2761.

30.   Jeng, J.-Y.; Chiang, Y.-F.; Lee, M.-H.; Peng, S.-R.; Guo, T.-F.; Chen, P.; Wen, T.-C. *Advanced Materials* **2013,** 25, (27), 3727-3732.

31.   Wang, J. T.; Ball, J. M.; Barea, E. M.; Abate, A.; Alexander-Webber, J. A.; Huang, J.; Saliba, M.; Mora-Sero, I.; Bisquert, J.; Snaith, H. J.; Nicholas, R. J. *Nano Lett* **2014,** 14, (2), 724-30.

32.   Liu, D.; Kelly, T. L. *Nature Photonics* **2013,** 8, (2), 133-138.

33.   Leijtens, T.; Eperon, G. E.; Pathak, S.; Abate, A.; Lee, M. M.; Snaith, H. J. *Nat Commun* **2013,** 4, 2885.

34.   Jeon, N. J.; Noh, J. H.; Kim, Y. C.; Yang, W. S.; Ryu, S.; Seok, S. I. *Nat Mater* **2014,** 13, (9), 897-903.

35.   Snaith, H. J.; Abate, A.; Ball, J. M.; Eperon, G. E.; Leijtens, T.; Noel, N. K.; Stranks, S. D.; Wang, J. T.-W.; Wojciechowski, K.; Zhang, W. *The Journal of Physical Chemistry Letters* **2014,** 5, (9), 1511-1515.

36.   Xiao, M.; Huang, F.; Huang, W.; Dkhissi, Y.; Zhu, Y.; Etheridge, J.; Gray-Weale, A.; Bach, U.; Cheng, Y. B.; Spiccia, L. *Angew Chem Int Ed Engl* **2014,** 53, (37), 9898-903.

37.   Kymakis, E.; Klapsis, G.; Koudoumas, E.; Stratakis, E.; Kornilios, N.; Vidakis, N.; Franghiadakis, Y. *Eur. Phys. J. Appl. Phys.* **2006,** 36, (3), 257-259.

38.   Park, H.; Chang, S.; Zhou, X.; Kong, J.; Palacios, T.; Gradecak, S. *Nano Lett* **2014,** 14, (9), 5148-54.

39.   Jeon, I.; Ryan, J. W.; Nakazaki, T.; Yeo, K. S.; Negishi, Y.; Matsuo, Y. *J. Mater. Chem. A* **2014,** 2, (44), 18754-18760.

40.   Park, H.; Shi, Y.; Kong, J. *Nanoscale* **2013,** 5, (19), 8934-8939.

41.   Yang, X.; Loos, J. *Macromolecules* **2007,** 40, (5), 1353-1362.

42.   Wang, Z.-S.; Kawauchi, H.; Kashima, T.; Arakawa, H. *Coordination Chemistry Reviews* **2004,** 248, (13–14), 1381-1389.

43.   Jaegermann, W.; Klein, A.; Mayer, T. *Advanced Materials* **2009,** 21, (42), 4196-4206.

44.   Thompson, C. V. *Annual Review of Materials Research, Vol 42* **2012,** 42, 399-434.

45.   Shin, D. W.; Lee, J. H.; Kim, Y. H.; Yu, S. M.; Park, S. Y.; Yoo, J. B. *Nanotechnology* **2009,** 20, (47), 475703.

46.   Jia, Y.; Cao, A.; Bai, X.; Li, Z.; Zhang, L.; Guo, N.; Wei, J.; Wang, K.; Zhu, H.; Wu, D.; Ajayan, P. M. *Nano Lett* **2011,** 11, (5), 1901-5.

47.   Shin, Y.-R.; Jeon, I.-Y.; Baek, J.-B. *Carbon* **2012,** 50, (4), 1465-1476.

48.   Shrotriya, V.; Li, G.; Yao, Y.; Chu, C.-W.; Yang, Y. *Applied Physics Letters* **2006,** 88, (7), 073508.

49.   Godoy, A.; Cattin, L.; Toumi, L.; Díaz, F. R.; del Valle, M. A.; Soto, G. M.; Kouskoussa, B.; Morsli, M.; Benchouk, K.; Khelil, A. *Solar Energy Materials and Solar Cells* **2010,** 94, (4), 648-654.

50.   Shiraishi, M.; Ata, M. *Carbon* **2001,** 39, (12), 1913-1917.

51.   Meyer, J.; Kidambi, P. R.; Bayer, B. C.; Weijtens, C.; Kuhn, A.; Centeno, A.; Pesquera, A.; Zurutuza, A.; Robertson, J.; Hofmann, S. *Sci Rep* **2014,** 4, 5380.

52.   Hellstrom, S. L.; Vosgueritchian, M.; Stoltenberg, R. M.; Irfan, I.; Hammock, M.; Wang, Y. B.; Jia, C.; Guo, X.; Gao, Y.; Bao, Z. *Nano Lett* **2012,** 12, (7), 3574-80.

53.   Stranks, S. D.; Eperon, G. E.; Grancini, G.; Menelaou, C.; Alcocer, M. J.; Leijtens, T.; Herz, L. M.; Petrozza, A.; Snaith, H. J. *Science* **2013,** 342, (6156), 341-4.

54.   Zuo, L.; Gu, Z.; Ye, T.; Fu, W.; Wu, G.; Li, H.; Chen, H. *Journal of the American Chemical Society* **2015,** 137, (7), 2674-2679.

55.   Zhao, Y.; Nardes, A. M.; Zhu, K. *Applied Physics Letters* **2014,** 104, (21), 213906.

Table of Contents Graphic and Synopsis
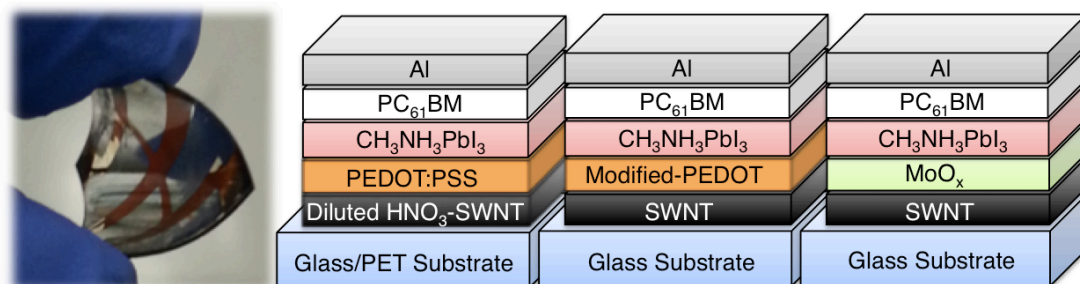
Supplementary Information

Single-walled Carbon Nanotube Film as Electrode in Indium-free Planar Heterojunction Perovskite Solar Cells: Investigation of Electron-blocking Layers and Dopants

Il Jeon,[†] Takaaki Chiba,[‡] Clement Delacou,[‡] Yunlong Guo,[†] Antti Kaskela,[§] Olivier Reynaud,[§] Esko I. Kauppinen,[§] Shigeo Maruyama,[‡] and Yutaka Matsuo[†]*

†: *Department of Chemistry, School of Science, The University of Tokyo, 7-3-1 Hongo, Bunkyo-ku, Tokyo 113-0033, Japan*

‡: *Department of Mechanical Engineering, School of Engineering, The University of Tokyo, 7-3-1 Hongo, Bunkyo-ku, Tokyo 113-8656, Japan*

§: *Department of Applied Physics, Aalto University School of Science, 15100, FI-00076 Aalto, Finland*

Contents:

1. Experimental

2. Crystal aggregation of perovskite film when fabricated on surfactant-PEDOT:PSS soaked SWNT substrate

3. Wettability observation and water contact angle test on various samples

4. *J-V* curves of the photovoltaic performance table 1

5. Photovoltaic performance of a nitric acid doped thicker SWNT-based perovskite SC

6. The energy band diagrams

7. Photovoltaic performance of MoO$_3$-utilized perovskite SCs

8. *J-V* curves of the photovoltaic performance table 2

9. Flexible application photovoltaic performance and cyclic flex test

10. *J-V* curves of flexible application and cyclic flex test

11. Pictures and cross-sectional SEM images of a flexible SWNT perovskite SC

12. Statistical analysis of the devices fabricated

1. Experimental

Aerosol SWCNT Preparation

SWCNTs were synthesized by an aerosol (floating catalyst) CVD method based on ferrocene vapor decomposition in a CO atmosphere. The catalyst precursor was vaporized by passing ambient temperature CO through a cartridge filled with ferrocene powder. The flow containing ferrocene vapor was then introduced into the high-temperature zone of a ceramic tube reactor through a water-cooled probe and mixed with additional CO. To obtain stable growth of SWCNTs, a controlled amount of CO_2 was added together with the carbon source (CO). SWCNTs were directly collected downstream of the reactor by filtering the flow through a nitrocellulose or silver membrane filter (Millipore Corp., USA; HAWP, 0.45 μm pore diameter).

SWNT electrode preparation

For the reference device, ITO substrates with size 15×15 mm^2 and an active area of 3×3 mm^2 with a sheet resistance of 6 Ω/square (Kuramoto Co., Ltd.) were sonicated in cleaning surfactant (Semi Clean, M-Lo), water, acetone and 2-isopropanol for 15 minutes each. The substrates were then dried in an oven at 70 °C. ITO substrates were exposed to UV/O$_3$ for 30 min in order to remove any remaining organic impurities.

For the SWCNT device, bare glass substrates (Kuramoto Co., Ltd.) were purchased and cleaned by the same method as the ITO substrates. Prior to SWCNT transfer, the substrates were exposed to UV/O$_3$ for 30 min. For the flexible device, Toyobo ltd. polyethylene terephthalate (A4300-38 μm) were used. The films were cleaned by ethanol and clean gauze.

SWCNT films were transferred onto the substrates by laminating from the top. A drop of ethanol was used to ensure firm adhesion of SWCNT. Then the substrates were transferred to a nitrogen filled glove box for further fabrication.

Modification of PEDOT:PSS

Surfactant-PEDOT:PSS was produced by adding 0.5 wt% of polyoxyethylene(6) tridecyl ether (Sigma Aldrich Chemical Co., Inc.) in poly-(3,4-ethylenedioxythiophene)-polystyrenesulfonic acid (PEDOT:PSS) dispersion in water (Clevios P VP, Heraeus Precious Metals GmbH & Co.). IPA-PEDOT:PSS was produced by diluting PEDOT:PSS in 2-isopropanol at 3:1(v/v) ratio. Modified PEDOT:PSS was spin coated at the same condition as the normal PEDOT:PSS which is 4500 rpm for 45 s.

MoO_3 Deposition

MoO_3 film was deposited under vacuum via a thermal evaporator. 15 nm MoO_3 was deposited with the average rate of 0.2 Å/s. For MoO_X doping, it was annealed at 300 °C for 3 h in N_2.

Perovskite Solution Preparation

The synthesized CH_3NH_3I (0.172 g) was mixed with PbI_2 (0.500 g) in anhydrous N,N-dimethylformamide (1.07 mL) by stirring at 60°C overnight to produce clear $CH_3NH_3PbI_3$ solution with a concentration of 45 wt%.

Inverted type planar heterojunction perovskite solar cell fabrication

PEDOT:PSS was spin coated at 300 rpm for 3 s and then 4500 rpm for 60 s on electrode substrate. In the case of MoO_3, 15nm thickness was thermally deposited under vacuum. $CH_3NH_3PbI_3$ solution (25 μL) was first dropped onto a PEDOT:PSS or MoO_3. The substrate was then spun at 4500 rpm and after eight seconds anhydrous chlorobenzene (10 μL) was quickly dropped onto the center of the substrate. This instantly changed the color of the substrate from transparent to light brown. The electron-transporting material was deposited by spin coating at 1500 rpm for 30 s. The spin coating solution was prepared by dissolving 20 mg of $PC_{61}BM$ in 1000 μL chlorobenzene. Device fabrication was finally

completed by thermal evaporation of a 70 nm thick film of aluminum as the cathode. Device fabrication was carried out in a N_2-filled glove box.

Normal type planar heterojunction perovskite solar cell fabrication

A 30 nm thick dense layer of TiO_2 was then coated on the ITO substrates by spin coating of a bis(isopropoxide)bis(acetylacetonato)titanium(IV) solution (75% in 2-propanol, Sigma-Aldrich) diluted in 2-propanol (1:9, volume ration) at 450 °C. To deposit perovskite films, the $CH_3NH_3PbI_3$ solution (25 μL) was first dropped onto a TiO_2. The substrate was then spun at 4500 rpm and after eight seconds anhydrous chlorobenzene (10 μL) was quickly dropped onto the center of the substrate. This instantly changed the color of the substrate from transparent to light brown. The hole-transporting material was deposited by spin coating at 1500 rpm for 30 s. The spin coating solution was prepared by dissolving 80 mg spiro-MeOTAD, 15 μL of a stock solution of 520 mg mL-1 lithium bis(trifluoromethylsulphonyl)imide in acetonitrile and 22.5 μL 4-tert-butylpyridine in 1 mL chlorobenzene. Device fabrication was finally completed by thermal evaporation of a 70-nm-thick film of silver as the cathode. Devices were left in a desiccator overnight and tested next day. Device fabrication was carried out in a N_2-filled glove box.

Characterizations

Current-voltage (J–V) characteristics were measured by software-controlled source meter (Keithley 2400) in dark conditions and 1 sun AM 1.5G simulated sunlight irradiation (100 mW/cm^2) using a solar simulator (EMS-35AAA, Ushio Spax Inc.), which was calibrated using a silicon diode (BS-520BK, Bunkokeiki). Topography images were recorded using an AFM operating in tapping mode (SPI3800N, SII). SEM measurement was carried out on S-4800 (Hitachi). Valence band information and Fermi levels were measured by Riken Keiki PYS-A AC-2 and kelvin probe spectroscopy in air (ESA), respectively. Both homemade systems based on Seki Technotron STR-250 (excitation wavelength 488nm) and inVia Raman microscope (Renishaw) were used for the Raman measurement. Shimadzu UV-3150 was used for the UV-vis-NIR measurement. Solartron SI1287 Electrochemical Interface and Solartron 1255B Frequency Reponse Analyzer were used for the Impedance measurement.

2. Crystal aggregation of perovskite film when fabricated on surfactant-PEDOT:PSS soaked SWNT substrate
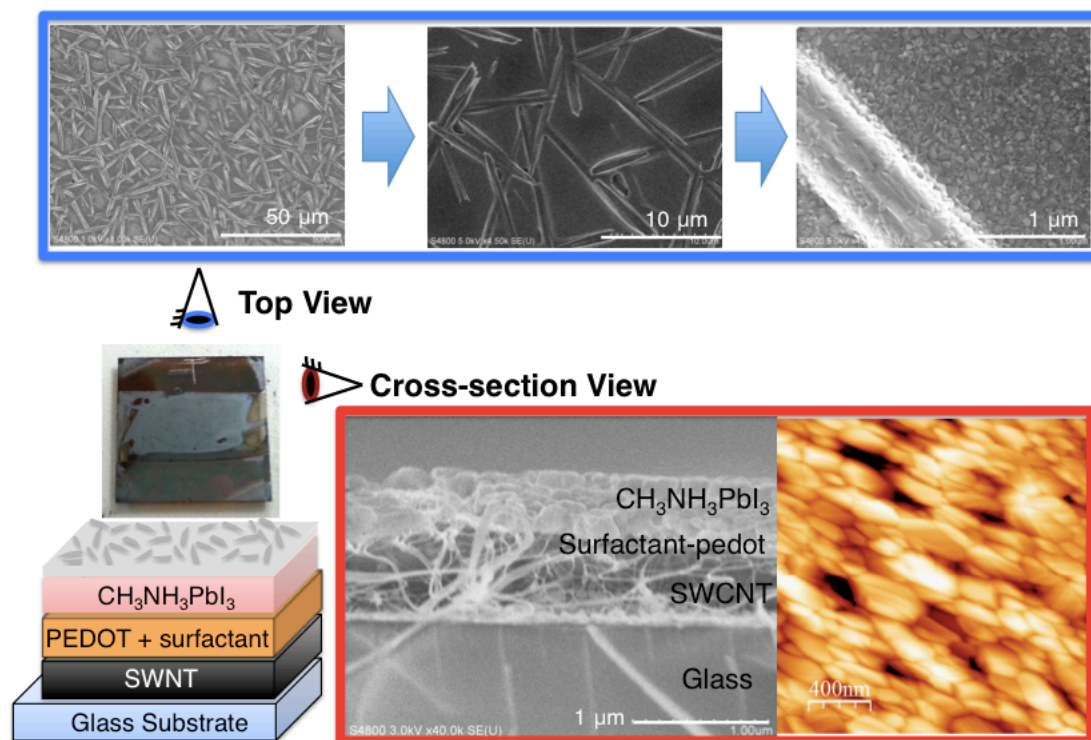

Figure S1. Top view and cross-sectional view of the Perovskite film on top of the surfactant-PEDOT:PSS-coated SWNT without shortening the CB rinsing time. The top view SEM images show magnification identifying the large aggregated crystals forming while the cross-sectional SEM shows a dissection of the aggregated perovskite layer.

3. Wettability observation and water contact angle test on various samples
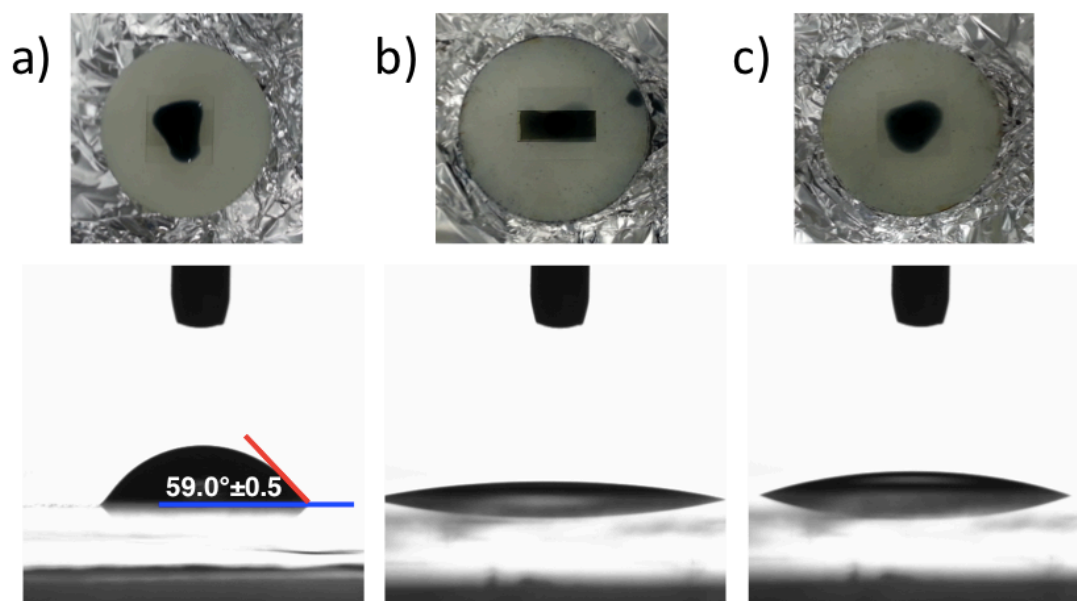
Figure S2. As cast wettability images (above) and water contact angle test on a) IPA-PEDOT:PSS on SWNT film on glass, b) surfactant-PEDOT:PSS on SWNT film on glass, and c) PEDOT:PSS on nitric acid 70 v/v%-treated SWNT film on glass.

4. *J-V* curves of the photovoltaic performance table 1
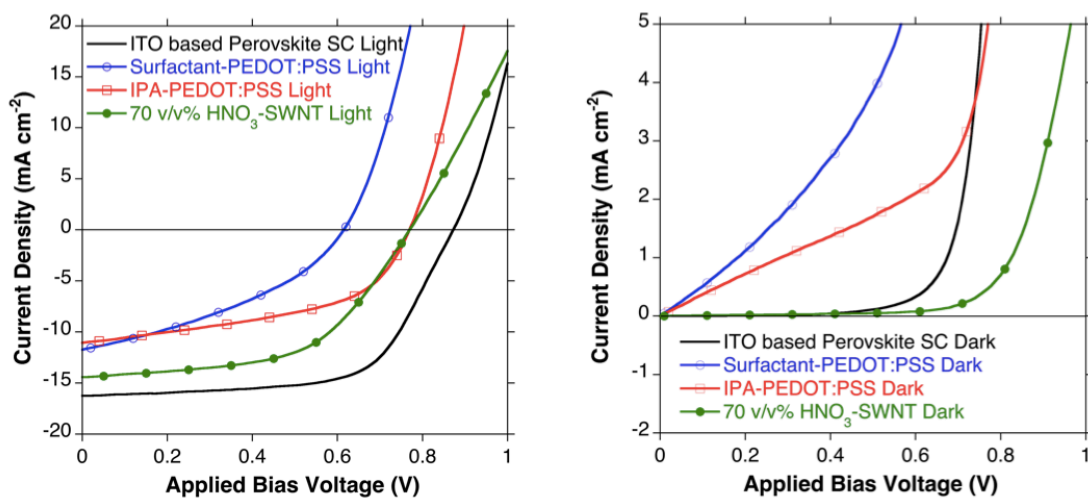
Figure S3-1. *J-V* curves of the ITO-based perovskite SC, the modified PEDOT:PSS-based perovskite SC, and the nitric acid-treated SWNT-based perovskite SC in light (left) and dark (right).
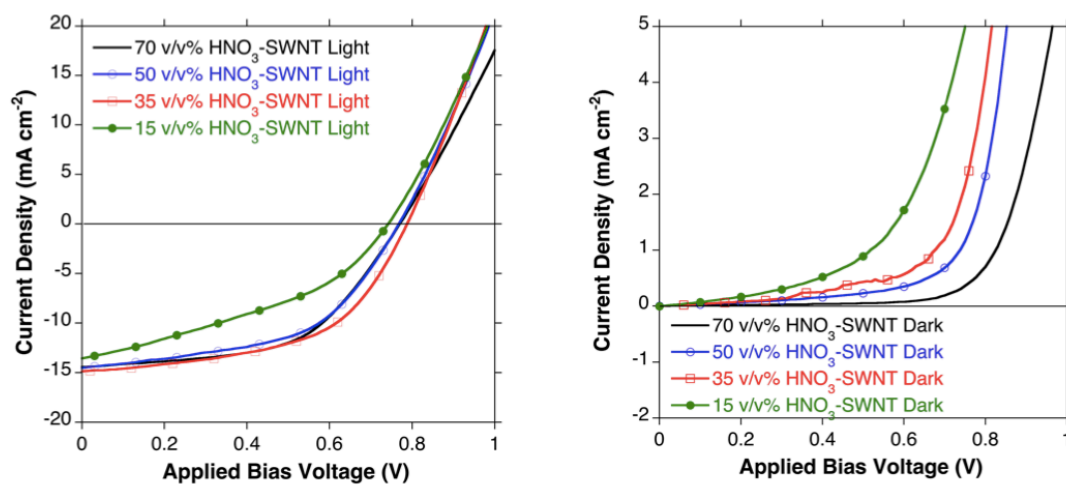
Figure S3-2. *J-V* curves of the perovskite SCs using nitric acid SWNTs with different concentrations in light (left) and dark (right).

5. Photovoltaic performance of a nitric acid doped thicker SWNT-based perovskite SC

Table S1. Photovoltaic performance of a nitric acid-doped thicker SWNT used perovskite SC.

Electrode	EBL	V_{OC} (V)	J_{SC} (mA/cm^2)	FF	R_S (Ωcm^2)	R_{SH} (Ωcm^2)	PCE (%)
70 v/v% HNO$_3$-SWNT	Surfactant-	0.56	11.5	0.37	100	2.9 x 10^3	2.37
ITO	PEDOT:PSS	0.89	14.9	0.61	98	6.5 x 10^3	8.03
Thicker SWNT doped by 70 v/v% HNO$_3$	PEDOT:PSS	0.87	10.5	0.61	95	7.13 x 10^3	5.62

6. The energy band diagrams
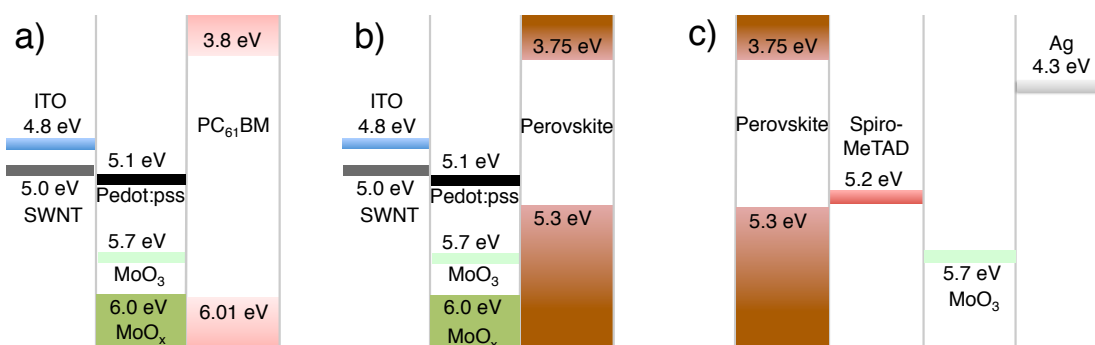
Figure S4. The energy band diagrams of a) organic SCs, b) inverted type perovskite SCs, and normal type perovskite SCs.

7. Photovoltaic performance of MoO₃-utilized perovskite SCs

Table S2. Photovoltaic performance of a nitric acid-doped thicker SWNT used perovskite SC.

Anode	V_{OC} (V)	J_{SC} (mA/cm^2)	FF	PCE (%)
SWNT/MoO₃/PEDOT:PSS	0.06	1.79	0.25	0.03
SWNT/IPA-PEDOT:PSS/MoO₃	0.07	0.77	0.25	0.02
MoO$_x$/SWNT/PEDOT:PSS	0.35	10.5	0.36	1.30
ITO	0.79	5.17	0.53	2.19

8. *J-V* curves of the photovoltaic performance table 2
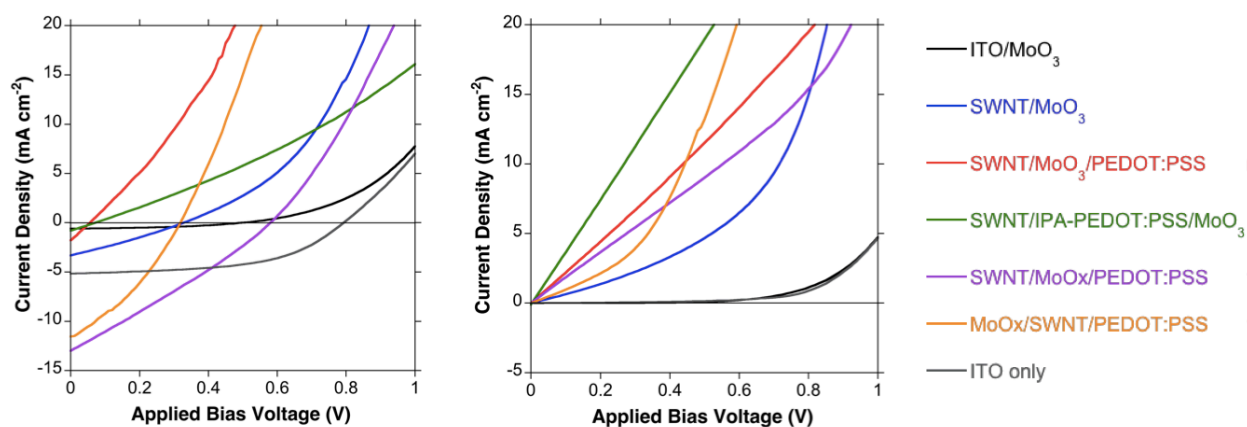
Figure S5-1. *J-V* curves of the perovskite SCs with various configurations involving MoO₃.
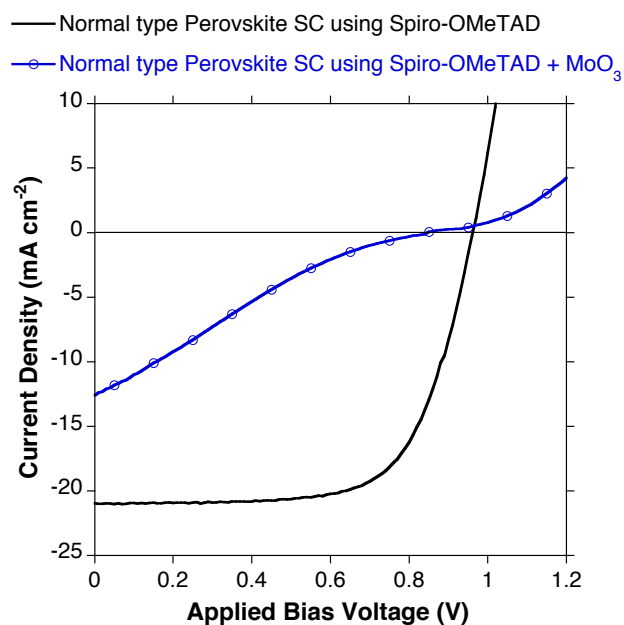
Figure S5-2. *J-V* curves of the normal type perovskite SCs with and without MoO$_3$.

9. Flexible application photovoltaic performance and cyclic flex test

Table S3. Photovoltaic performance of a flexible SWNT Perovskite SC and after 10 mm curvature cyclic flex was applied.

Electrode	V_{OC} (V)	J_{SC} (mA/cm^2)	FF	R_S (Ωcm^2)	R_{SH} (Ωcm^2)	PCE (%)
Flexible	0.81	11.8	0.56	105	6.05 x 10^3	5.38
After cyclic flex test	0.79	11.5	0.50	135	4.22 x 10^3	4.60

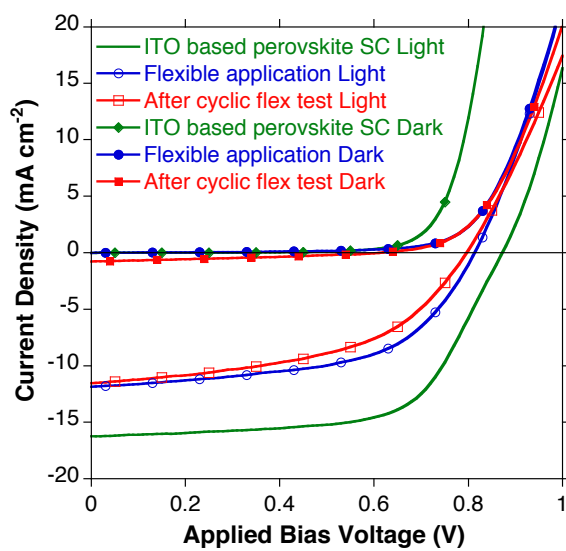## 10. *J-V* curves of flexible application and cyclic flex test

Figure S6. *J-V* curves of the perovskite SCs using nitric acid SWNTs with different concentrations in light (left) and dark (middle). The legend is on the right.

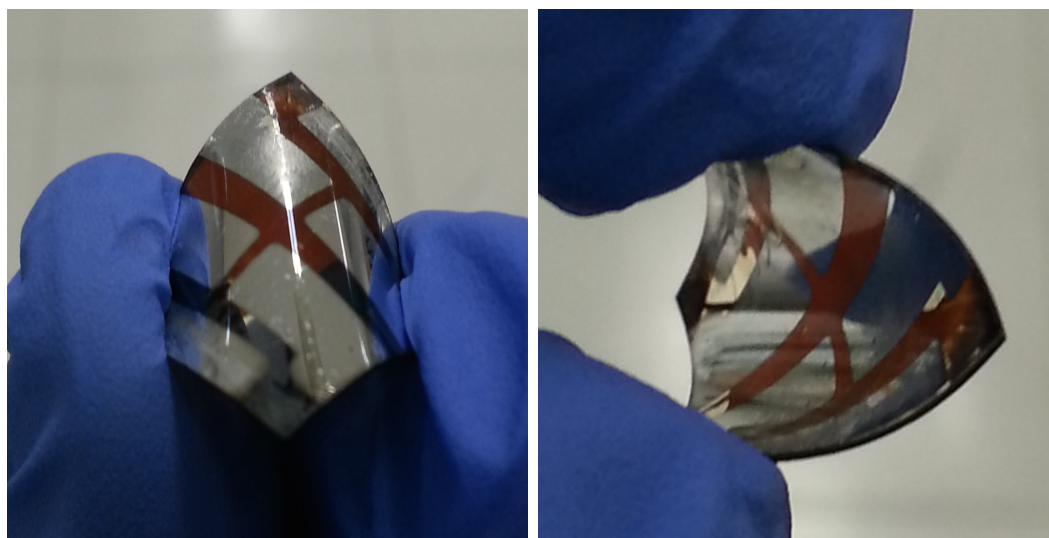## 11. Pictures and cross-sectional SEM images of a flexible SWNT perovskite SC

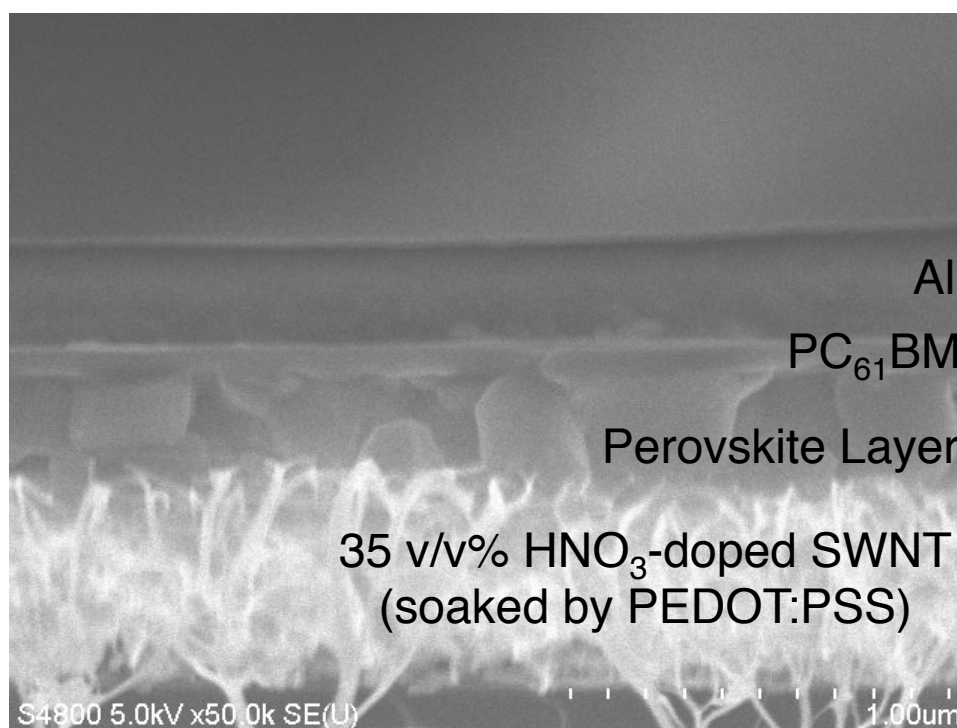**Figure S8-1.** Pictures of a HNO$_3$ (35 v/v%)-doped SWCNT-based flexible perovskite SCs.

Figure S8-2. A cross-sectional SEM image of a HNO$_3$ (35 v/v%)-doped SWCNT-based flexible perovskite SC.

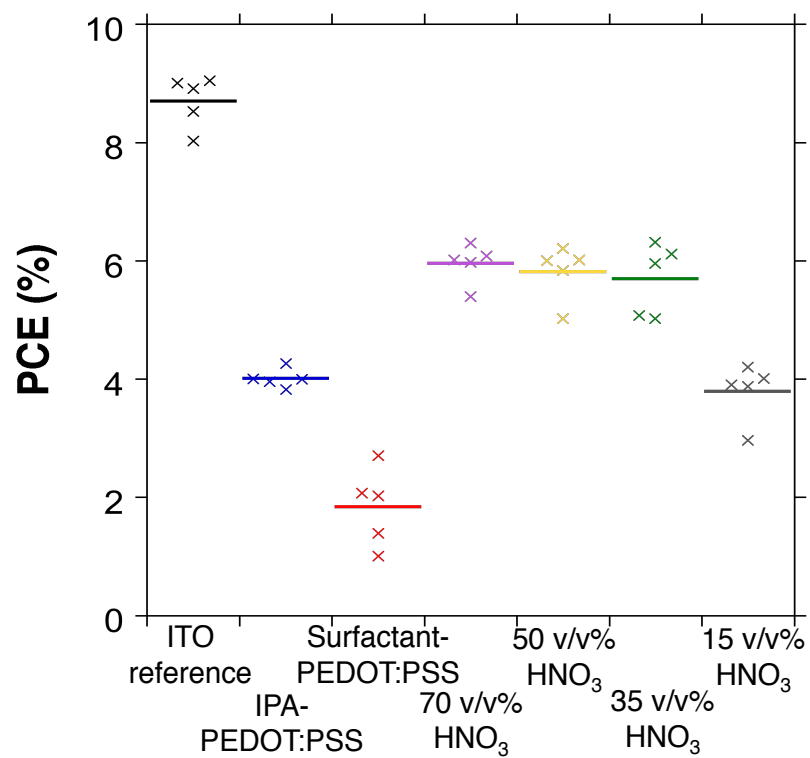## 12. Statistical analysis of the devices fabricated

Figure S9. A statistical data graph illustrating reproducibility of the perovskite SCs in this work. Crosses represent each device performance and bars represent averages.